



# Dark and Dronc activation in *Drosophila melanogaster*

Lu Tian<sup>a</sup> , Yini Li<sup>a,1</sup> , and Yigong Shi<sup>a,b,c,d,1</sup>

Edited by Hao Wu, Harvard Medical School, Boston, MA; received July 26, 2023; accepted January 19, 2024

The onset of apoptosis is characterized by a cascade of caspase activation, where initiator caspases are activated by a multimeric adaptor complex known as the apoptosome. In *Drosophila melanogaster*, the initiator caspase Dronc undergoes autocatalytic activation in the presence of the Dark apoptosome. Despite rigorous investigations, the activation mechanism for Dronc remains elusive. Here, we report the cryo-EM structures of an auto-inhibited Dark monomer and a single-layered, multimeric Dark/Dronc complex. Our biochemical analysis suggests that the auto-inhibited Dark oligomerizes upon binding to Dronc, which is sufficient for the activation of both Dark and Dronc. In contrast, the previously observed double-ring Dark apoptosome may represent a non-functional or “off-pathway” conformation. These findings expand our understanding on the molecular mechanism of apoptosis in *Drosophila*.

apoptosis | Dark | Dronc | cryo-EM

Apoptosis is indispensable in metazoans (1–3). The conserved apoptosis regulatory pathways have been delineated in several model organisms, including *Caenorhabditis elegans*, *Drosophila melanogaster*, and mammals (1). In general, the onset of apoptosis involves a cascade of proteolytic activation of both initiator and effector caspases (4, 5). The autocatalytic activation of initiator caspases entails a multimeric adaptor complex, usually referred to as the apoptosome (6). Effector caspases are activated through direct proteolytic cleavage by the initiator caspases (4).

In *D. melanogaster*, the initiator caspase Dronc is suppressed by *Drosophila* inhibitor of apoptosis (DIAP)-mediated ubiquitination (7–9). Upon apoptotic stimuli, DIAP is antagonized by the pro-apoptotic proteins Reaper, Hid, and Grim (RHG) (7–9). Facilitated by Dark through a conserved interaction between their respective caspase recruitment domains (CARDs), Dronc undergoes autocatalytic cleavage (10–13). Unlike the mammalian initiator caspase-9, which remains associated with the Apaf-1 apoptosome to function as a holoenzyme (14), activated Dronc dissociates from the Dark apoptosome and autonomously cleaves the downstream effector caspase DrICE (15).

Under non-apoptotic condition, Dark exists as an auto-inhibited monomer (13). In contrast to its mammalian orthologue Apaf-1, which requires dATP and cytochrome *c* (Cyt *c*) for oligomerization (14, 16, 17), Dark activation is independent of Cyt *c* (18–20). In the presence of dATP, 16 Dark protomers assemble into a double-ring complex, as revealed by the cryo-EM structure of the Dark apoptosome (13, 21). In vitro biochemical studies showed that Dronc-CARD or full-length (FL) Dronc zymogen is sufficient to induce Dark oligomerization for Dronc activation even in the absence of exogenous nucleotides (13). Intriguingly, the complex of Dark bound to Dronc-CARD also exists as a double ring, with 16 CARDs sandwiched by two rings of Dark, each comprising eight Dark protomers (13). In addition, upon activation, Dark and Dronc were reported to form a single ring, although the structure remains to be elucidated (22). Despite these advances, the molecular mechanism by which Dark and Dronc are activated remains poorly understood. In particular, the function of the Dark and Dark/Dronc-CARD double rings is unclear.

To address these questions, we solved the structure of the auto-inhibited Dark, reasoning that its comparison with the oligomeric Dark would explain the dispensability of dATP for Dark oligomerization in the presence of Dronc-CARD or FL-Dronc (13). We also determined the structure of Dark in the presence of FL-Dronc to understand the molecular basis of Dark-facilitated Dronc activation.

Through structural analysis, we show that the conformational changes associated with Dark oligomerization are similar to those observed in Apaf-1. Dark in the presence of FL-Dronc assembles into an unsealed ring, much like a helical spiral. Our biochemical studies suggest that the previously characterized double-ring Dark apoptosome may represent an off-pathway state. The interaction between Dark and Dronc per se is sufficient to activate both proteins. These findings demonstrate both evolutionary conservation as well as key deviations of apoptosis in different organisms.

## Significance

Apoptosis is triggered by initiator caspase activation, which is thought to rely on a multimeric machinery known as the apoptosome. The initiator caspase-9 in mammals is activated by the Apaf-1 apoptosome. Similarly, Dronc in *Drosophila* is thought to be activated by the Dark apoptosome. The molecular mechanism by which an initiator caspase is activated by its corresponding apoptosome remains elusive. In this study, we provide key insights into how Dark mediates Dronc activation. Quite unexpectedly, Dark and Dronc form a single-layered, unsealed ring, which is sufficient for Dronc activation. This conclusion may have important implications for caspase-9 activation.

Author affiliations: <sup>a</sup>Beijing Frontier Research Center for Biological Structures, Tsinghua-Peking Center for Life Sciences, School of Life Sciences, Tsinghua University, Beijing 100084, China; <sup>b</sup>Westlake Laboratory of Life Sciences and Biomedicine, Westlake Institute for Advanced Study, Hangzhou 310024, China; <sup>c</sup>Key Laboratory of Structural Biology of Zhejiang Province, School of Life Sciences, Westlake University, Hangzhou 310024, China; and <sup>d</sup>Institute of Biology, Westlake Institute for Advanced Study, Hangzhou 310024, China

Author contributions: L.T., Y.L., and Y.S. designed research; L.T. and Y.L. performed research; L.T., Y.L., and Y.S. analyzed data; and L.T., Y.L., and Y.S. wrote the paper.

The authors declare no competing interest.

This article is a PNAS Direct Submission.

Copyright © 2024 the Author(s). Published by PNAS. This article is distributed under Creative Commons Attribution-NonCommercial-NoDerivatives License 4.0 (CC BY-NC-ND).

<sup>1</sup>To whom correspondence may be addressed. Email: li\_yini@163.com or syg@westlake.edu.cn.

This article contains supporting information online at <https://www.pnas.org/lookup/suppl/doi:10.1073/pnas.2312784121/-DCSupplemental>.

Published February 21, 2024.

## Results

**Structure of the Auto-Inhibited Dark Monomer.** Recombinant Dark was expressed and purified following a published protocol (13). When the purified protein was applied to size exclusion chromatography (SEC), we observed concentration-dependent oligomerization, which is consistent with a previous study (22). At a low concentration of approximately 0.5  $\mu$ M, Dark was eluted at a volume that corresponds to the molecular weight of a monomer (*SI Appendix*, Fig. S1A, blue line). However, at a slightly higher concentration of 1  $\mu$ M, Dark began to oligomerize into a much larger complex (*SI Appendix*, Fig. S1A, magenta line). To help maintain Dark in a monomeric, auto-inhibited state, we introduced a missense mutation D333A, which targets Asp333 at the oligomeric interface. Indeed, Dark (D333A) exists mostly as a monomer even at 2  $\mu$ M concentration (*SI Appendix*, Fig. S1B). We used Dark (D333A) to prepare cryo-EM samples using graphene-covered grids. Most of the particles on the EM micrograph correspond to monomeric Dark (*SI Appendix*, Fig. S1C).

We determined the cryo-EM structure of the Dark (D333A) monomer at an average resolution of 3.9  $\text{\AA}$ , with the core region

at approximately 3.5  $\text{\AA}$  (Fig. 1A and *SI Appendix*, Fig. S1 C–F and Table S1). An extra EM density is clearly present in the region of nucleotide-binding site, albeit at a relatively low resolution. Through mass spectrometric analysis, the wild-type (WT) Dark monomer was found to contain mostly ADP after SEC (*SI Appendix*, Fig. S2 A and B). Therefore, we modeled an ADP molecule based on the crystal structure of auto-inhibited Apaf-1 (PDB code: 1Z6T) (23). The structure of Dark (D333A) sequentially contains a CARD at the N terminus, a nucleotide-binding domain (NBD), a helical domain (HD1), a winged-helix domain (WHD), a second helical domain (HD2), and two WD40 domains at the C terminus (Fig. 1A). The overall architecture of the auto-inhibited Dark (D333A) monomer resembles that of the auto-inhibited Apaf-1, with the NBD stacking against the WDs for the maintenance of the auto-inhibited state (23) (*SI Appendix*, Fig. S2 C and D).

Compared to auto-inhibited Apaf-1, the corresponding domains within auto-inhibited Dark (D333A) are more loosely packed together and the bound ADP is more accessible to solvent, which may account for the moderate resolution of the nucleotide in our structure. The interfaces of NBD/WD1 and HD2/WD1

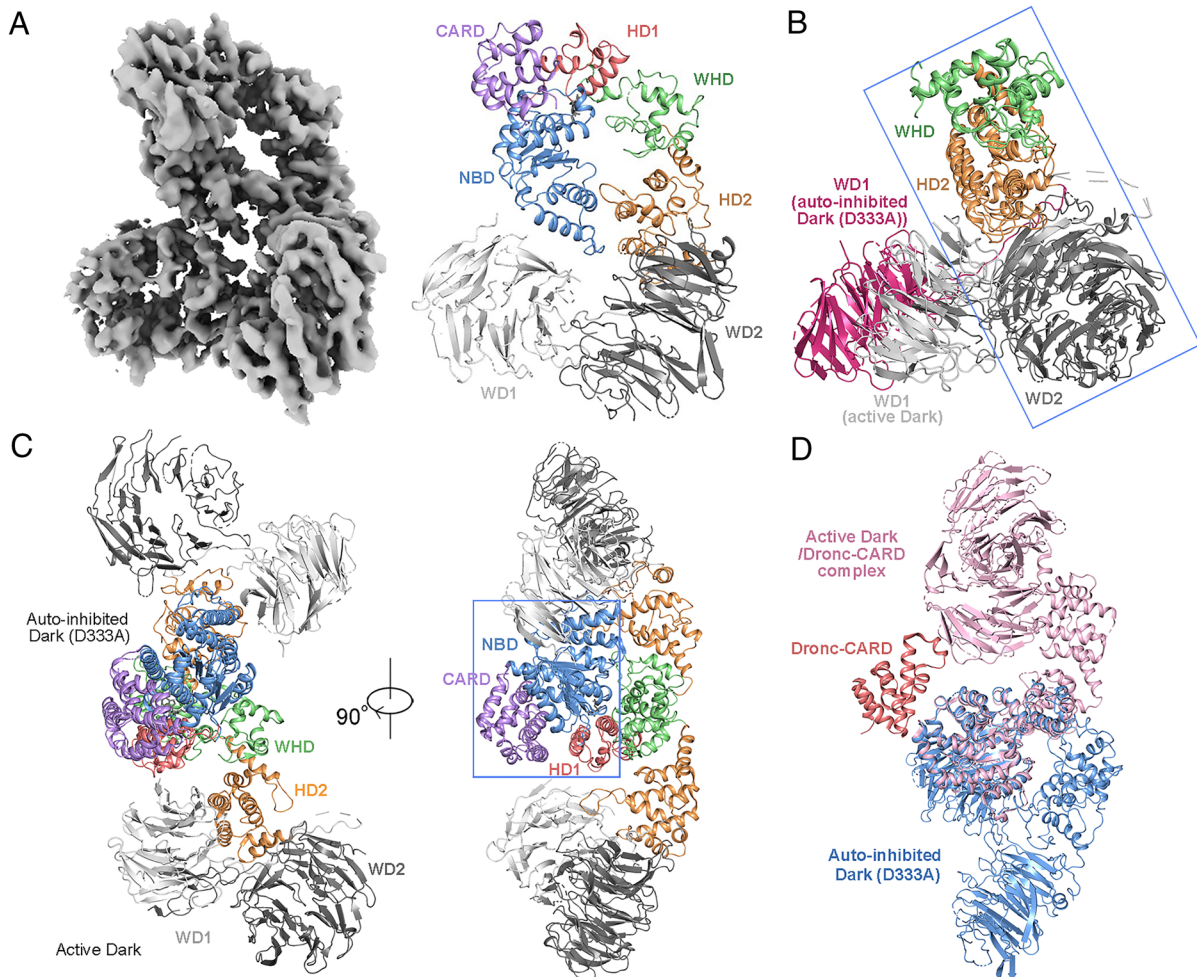


**Fig. 1.** Cryo-EM structure of an auto-inhibited Dark (D333A) monomer. (A) The overall EM map (Left) and the structure (Right) of the auto-inhibited Dark (D333A) monomer. (B) Structural comparison between the auto-inhibited Dark (D333A) monomer and the Dark protomer from the Dark apoptosome (PDB code: 3J9L) based on alignment of WHD. The rigid WHD-HD2-WD2 rod is indicated by the blue rectangular box. (C) Structural comparison between the auto-inhibited Dark (D333A) monomer and the Dark protomer from the Dark apoptosome (PDB code: 3J9L) based on alignment of NBD and HD1 (indicated by the blue rectangle in the Right panel). Upon the formation of the Dark apoptosome, the WHD-HD2-WD2 rod is rotated by  $\sim 180^\circ$ . (D) The binding interface for Dronc-CARD is exposed in the auto-inhibited Dark (D333A) monomer. The structures of the auto-inhibited Dark (D333A) (light blue) and the Dark protomer (light pink) from the Dark/Dronc-CARD complex are aligned on the basis of NBD. Dronc-CARD is colored orange.

in Apaf-1 are thought to be essential for maintaining autoinhibition (24) (*SI Appendix*, Fig. S2 D, Left). In contrast, these domains are loosely connected in the auto-inhibited Dark (D333A) (Fig. 1A). Such loose association may contribute to the moderate resolution and the high flexibility of WD1 observed during data processing (*SI Appendix*, Fig. S1C). Dark (D333A) autoinhibition is mainly mediated by the interactions between NBD and HD2 and the putative interacting residues are identified (*SI Appendix*, Fig. S2 D, Right).

Dark undergoes marked domain rearrangements during oligomerization. Structural comparison between the Dark protomer from the double-ring Dark apoptosome (PDB code: 3J9L) and the auto-inhibited Dark (D333A) identifies two rigid bodies. The first is the conserved WHD–HD2–WD2 rod, analogous to that in Apaf-1 (24) (Fig. 1B, blue rectangle). The second involves the CARD, NBD, and HD1 (Fig. 1C, blue rectangle). Upon oligomerization, these two rigid bodies rotate approximately 180° relative to each other (Fig. 1C). Notably, the binding interface for Dronc-CARD is fully accessible in the auto-inhibited Dark (D333A) (Fig. 1D). This structural feature nicely explains why

Dronc may directly activate the auto-inhibited Dark through direct interaction.

**Structure of the Dark/Dronc Complex.** Dronc activation involves two essential cleavages: one after Glu143, which demarcates the CARD and the catalytic domain; and the other after Glu352, which separates the large and small subunits of the catalytic domain. In addition, Dronc is susceptible to proteolytic cleavages at Asp113 and Glu135. Cys318 is the catalytic residue in Dronc. To prevent Dronc cleavage, we introduced four missense mutations (D113A, E135A, E143A, and E352A) into the catalytic mutant Dronc (C318A). The resulting Dronc variant (named 4M) was incubated with the auto-inhibited Dark to assemble into an active complex, which presumably mimics the intermediate state during Dronc activation.

Notably, the Dark/Dronc (4M) complex exhibits a markedly smaller molecular mass compared to the double-ring Dark apoptosome (Fig. 2A and *SI Appendix*, Fig. S3A), which is in agreement with previous findings (22). This complex was subjected to cryo-EM analysis (*SI Appendix*, Fig. S3 B–E and Table S1). A large

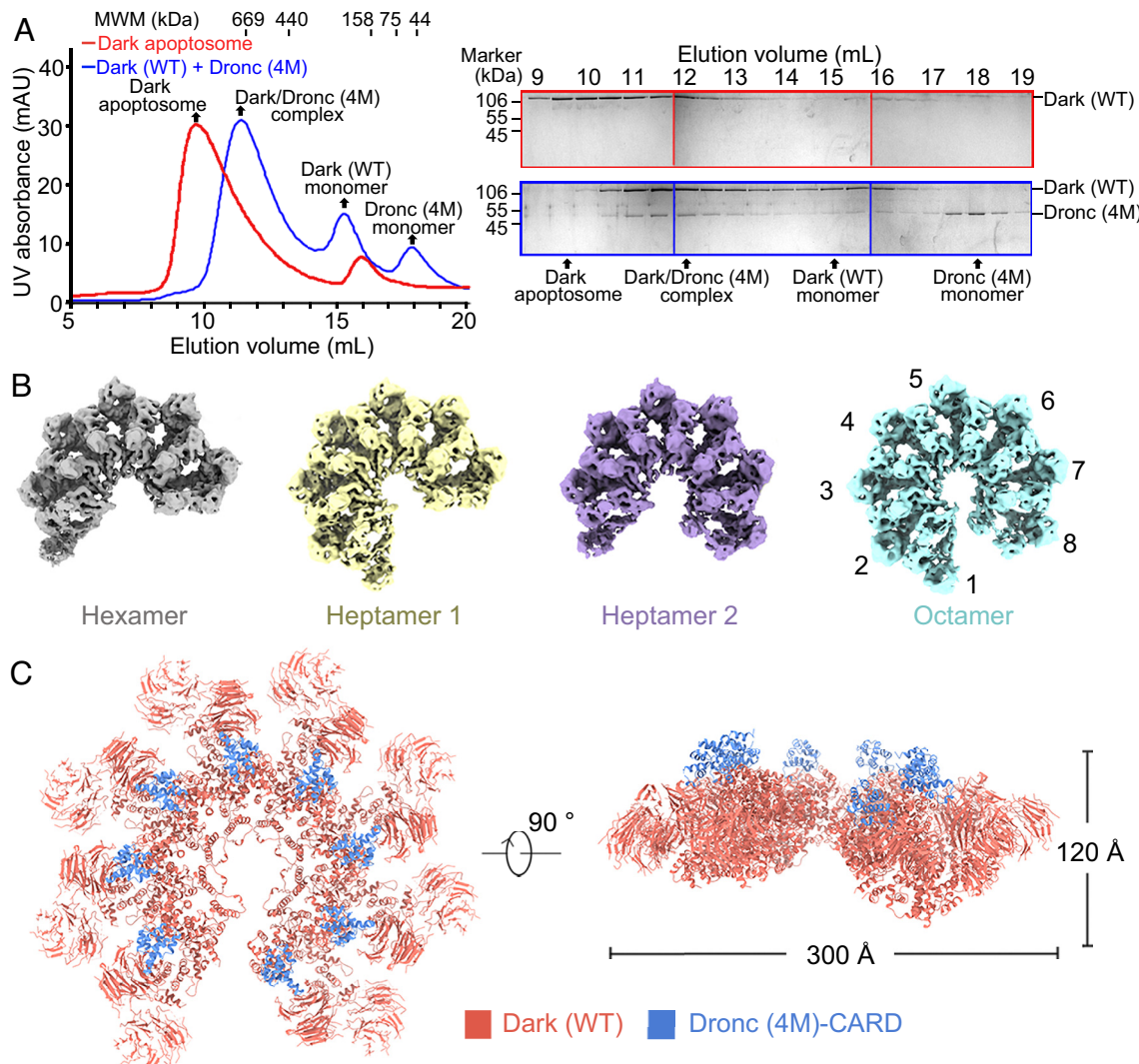


**Fig. 2.** Cryo-EM structure of the Dark/Dronc (4M) complex. (A) The auto-inhibited Dark monomer and Dronc (4M) assemble into a multimeric complex. This complex displays a smaller molecular mass compared to the Dark apoptosome. The peak fractions of the SEC chromatograms (Left) were visualized on SDS-PAGE using Coomassie blue staining (Right). (B) The overall EM reconstructions of the Dark/Dronc (4M) complex. Shown here are the overall EM maps of a hexamer (gray), two heptamers (yellow and purple), and an octamer (cyan). Protomers are numbered in the octamer. (C) Two perpendicular views of the octameric Dark/Dronc (4M) complex. Eight Dark molecules (salmon) and eight Dronc-CARDs (cornflower) were docked into the EM map of the Dark/Dronc (4M) complex to generate this model.

majority of the particles display the appearance of an unsealed single ring, or partial helical spiral (*SI Appendix*, Fig. S3B). This appearance is markedly different from the double-ring Dark apoptosome. Through 3D classification and refinement, we obtained four distinct EM reconstructions: a hexamer, two heptamers (heptamer 1 and 2), and an octamer with C1 symmetry (Fig. 2B and *SI Appendix*, Fig. S3B). In all four EM reconstructions, the density corresponding to the Dronc catalytic domain fails to be observed, presumably due to its highly flexible connection to the unsealed ring. These four structures share a similar architecture (Fig. 2B). Subsequent discussion will mainly focus on the octamer.

Structure of the octameric Dark/Dronc (4M) complex displays a single-layered unsealed ring, with two terminal protomers (protomers 1 and 8) flexibly associated. The overall resolution for the reconstruction of the octameric complex is 7.0 Å (*SI Appendix*, Fig. S3B), which enables the docking of the Dark/Dronc-CARD complex (PDB code: 3J9K) into our EM map. The final model includes eight Dark molecules and eight Dronc-CARDs, arranged into an unsealed ring with a diameter of ~300 Å and a height of ~120 Å (Fig. 2C). Similar to that observed in the structure of the double-ring Dark/Dronc-CARD complex (13), Dronc-CARD simultaneously interacts with Dark-CARD and the WD40 repeats of Dark (Fig. 2C), which is essential for the assembly of the multimeric Dark/Dronc complex. The catalytic domain of Dronc (4M) has little EM density, likely due to its flexible linkage to its CARD. This observation also indicates that the Dronc catalytic domain has no stable interaction with Dark.

The eight Dark protomers of the unsealed ring are not in the same plane. This feature is quite clear upon aligning the terminal protomer of this unsealed ring with a protomer of the single ring derived from the double-ring Dark apoptosome (PDB code: 3J9L) (Fig. 3A, Top). Next, a representative helix (residues 217 to 230) located within the NBD, a region with higher resolution, was used to compare the unsealed ring with the single-ring Dark apoptosome (Fig. 3A, Lower). Intriguingly, there is a notable increase in the diameter of the unsealed Dark ring compared to that of the Dark apoptosome (Fig. 3A, Lower). The unsealed ring is distorted like an incomplete helical spiral. We aligned the first Dark protomer of one unsealed octamer onto the eighth Dark protomer of another unsealed octamer (Fig. 3B). This operation results in the generation of ~1.7 helical turns, which have a diameter of about 300 Å and a helical pitch of ~55 Å (Fig. 3B).

Similar to the sealed Dark apoptosome, the formation of the unsealed Dark ring relies on the interface between two

neighboring Dark protomers. This interface mainly involves two adjacent NBDs. Compared to the sealed Dark apoptosome (*SI Appendix*, Fig. S4A), the two NBDs between two adjacent Dark protomers in the unsealed Dark ring are slightly separated (*SI Appendix*, Fig. S4B). For example, with a distance of 4.0 Å, Leu217 of one Dark protomer makes van der Waals contacts to the aliphatic side chain of Glu194 from the adjacent Dark protomer in the sealed Dark apoptosome (*SI Appendix*, Fig. S4A). However, this distance becomes 7.2 Å, making such interactions highly unlikely (*SI Appendix*, Fig. S4B). Similarly, at a distance of 2.6 Å, Asp14 of one Dark protomer accepts a hydrogen bond (H-bond) from Arg142 of the adjacent Dark protomer in the sealed Dark apoptosome (*SI Appendix*, Fig. S4A). This distance becomes 3.5 Å, markedly weakening the intended H-bond. The weaker interface among adjacent protomers of the unsealed Dark ring is consistent with its observed flexibility.

**The Sealed Dark Apoptosome Fails to Activate Dronc.** FL Dronc and the auto-inhibited Dark monomer spontaneously assemble into a multimeric complex, within which Dronc becomes enzymatically activated (13). This observation prompted us to investigate the role of the double-ring Dark apoptosome in Dronc activation. The assembly of the Dark apoptosome in vitro requires high concentrations of dATP (5 to 10 mM) and Dark, which are non-physiological (20, 22, 25). To evaluate the assembly efficiency of the Dark apoptosome, we incubated the auto-inhibited Dark monomer (10 µM) with varying concentrations of dATP, followed by SEC analysis. At a low concentration of dATP (20 µM), the vast majority of the auto-inhibited Dark monomers remain monomeric (Fig. 4A). Even at 5 mM dATP, no more than half of the auto-inhibited Dark monomers were assembled into the Dark apoptosome (Fig. 4A). Therefore, the auto-inhibited Dark monomers are unlikely to form the Dark apoptosome under physiological conditions.

We investigated whether the double-ring Dark apoptosome can recruit Dronc. Dronc (4M) was incubated with the pre-assembled Dark apoptosome, and the mixture was analyzed by SEC. Much to our surprise, the pre-assembled Dark apoptosome fails to form a complex with Dronc, as shown by the inability of Dronc to co-migrate with the Dark apoptosome (Fig. 4B, orange line). Next, Dronc (4M) was incubated with the auto-inhibited Dark monomer and the mixture was analyzed by SEC. Dronc (4M) and Dark formed a distinct complex, which has a molecular weight smaller than that of the Dark apoptosome (Fig. 4B, blue line).

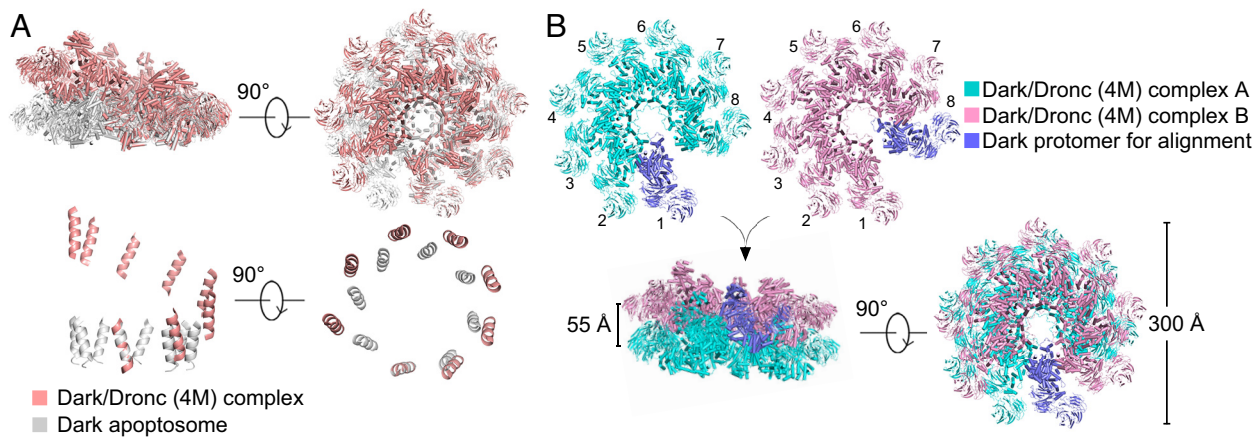


**Fig. 3.** The Dark/Dronc (4M) complex forms an unsealed single-ring structure. (A) Structural alignment of the Dark apoptosome (gray) and the Dark/Dronc (4M) complex (salmon) (Upper). Helices (residues 217 to 230) from the Dark NBDs are shown (Lower). (B) Features of the unsealed Dark single ring. Protomer 1 from one unsealed single ring is aligned with protomer 8 from another unsealed single ring to generate a helical spiral, which has a diameter of 300 Å and a helical pitch of 55 Å.

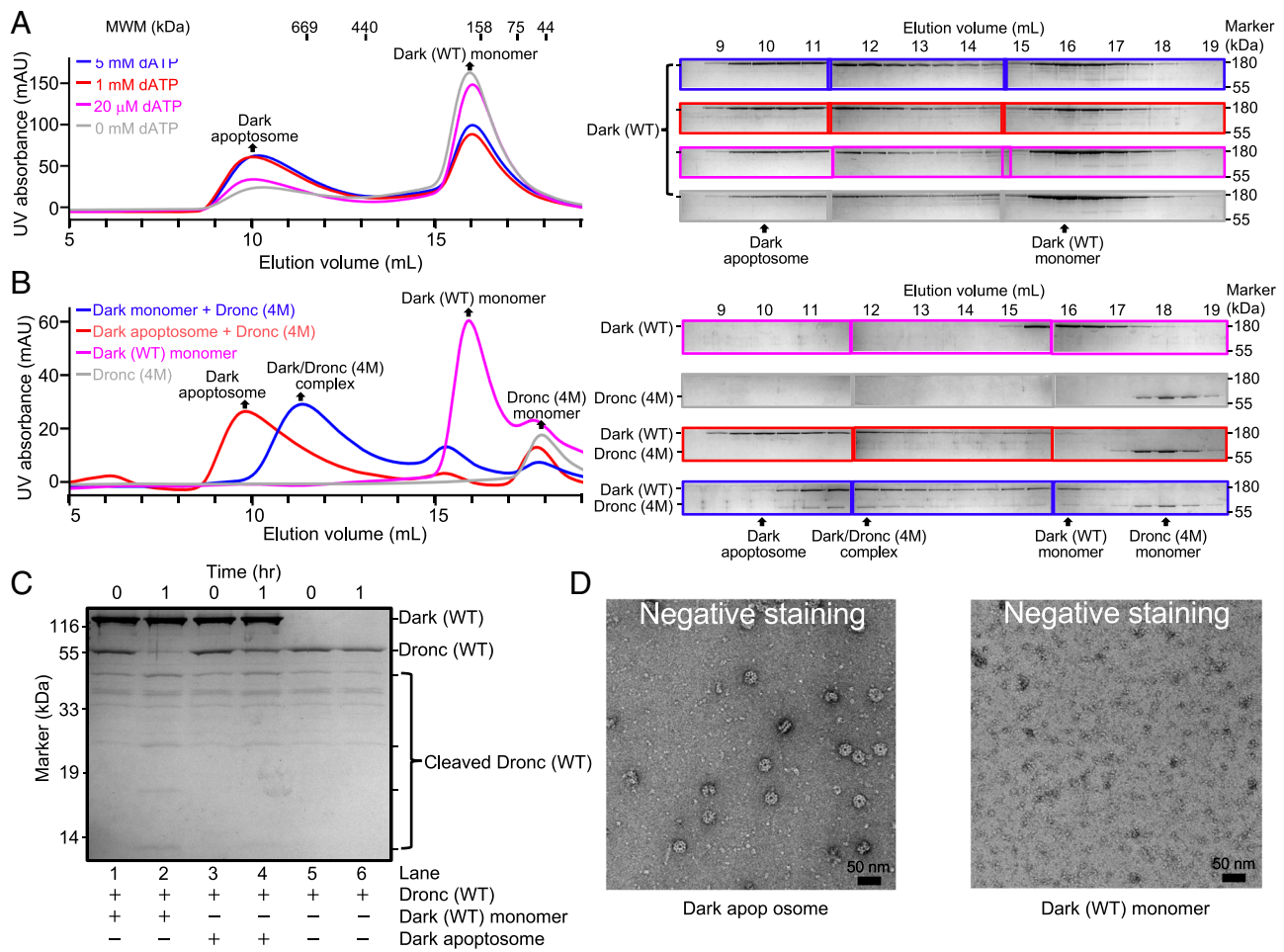


**Fig. 4.** The double-ring Dark apoptosome may represent an off-pathway state. (A) Assembly of the Dark apoptosome requires high concentrations of dATP. Assembly of the Dark apoptosome under varying concentrations of dATP was examined using SEC. The peak fractions of the SEC chromatograms (Left) were visualized on SDS-PAGE using Coomassie blue staining (Right). (B) The auto-inhibited Dark monomer binds to Dronc (4M) more efficiently than the Dark apoptosome. Dronc (4M) was incubated with the pre-assembled Dark apoptosome or the auto-inhibited Dark monomer. The peak fractions of the SEC chromatograms (Left) were visualized on SDS-PAGE using Coomassie blue staining (Right). (C) Autocatalytic cleavage of Dronc zymogen is greatly facilitated by the auto-inhibited Dark monomer but not by the Dark apoptosome. (D) Representative Negative staining images of the Dark apoptosome (Left) and the auto-inhibited Dark monomer (Right). Scale bar is marked on the image.

This complex, with its SEC elution peak characteristic of more than one species, presumably corresponds to the Dronc-Dark unsealed rings (Fig. 2B).

In agreement with the above analysis, WT Dronc zymogen underwent autocatalytic activation in the presence of the auto-inhibited Dark monomer (Fig. 4C, lanes 1 and 2) but not in the presence of the pre-assembled Dark apoptosome (Fig. 4C, lanes 3 and 4). To ensure the integrity of the Dark apoptosome during these assays, we used negative staining EM to characterize the Dark apoptosome, which indeed remains intact (Fig. 4D). Nonetheless, in the case of disassembly, the Dark monomers may be used to activate Dronc through formation of the unsealed Dark ring. Such disassembly may account for the contradictory findings reported previously (13). Taken together, these results suggest that formation of the double-ring Dark apoptosome might not be required for Dronc activation or apoptosis initiation in *Drosophila*.

## Discussion

In this study, we determined the cryo-EM structure of an auto-inhibited Dark (D333A) monomer, which through comparison with the Dark apoptosome reveals a set of conserved structural rearrangements required for Dark oligomerization. Compared to

the auto-inhibited Apaf-1 monomer, Dark exhibits two distinguishing and functionally important features. First, the WD1/NBD and WD1/HD2 interfaces, which are pivotal for maintenance of the auto-inhibited state, involve considerably less interactions in the Dark (D333A) monomer compared to Apaf-1. Second, the domains NBD, HD1, WHD, and HD2 in Dark are more loosely associated with one another than in Apaf-1. Accordingly, the bound ADP in Dark is more accessible to solvent than in Apaf-1. These structural features corroborate the empirical finding that Dark is more readily activated than Apaf-1.

We also assembled the Dark/Dronc (4M) complex using an uncleavable Dronc (4M) to mimic the intermediate state prior to Dark-facilitated Dronc autocatalytic cleavage. This complex has an unusual structure of an unsealed single ring, within which Dronc (4M) interacts with Dark through their conserved CARD/CARD interface. Our associated biochemical analysis strongly argues that the double-ring Dark apoptosome may represent an off-pathway state. First, the assembly depends on non-physiological concentrations of dATP. Second and more importantly, the auto-inhibited Dark monomer and the Dronc zymogen assemble into an unsealed ring, within which Dronc is activated. But Dronc zymogen can hardly be activated by the assembled Dark apoptosome in vitro.

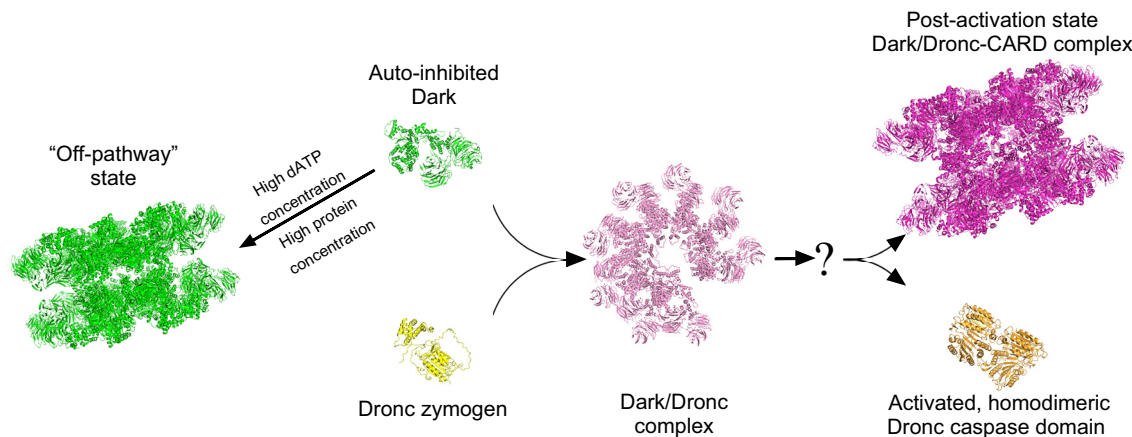


**Fig. 5.** A working model for Dark facilitated Dronc activation. Dark is initially expressed as an auto-inhibited monomer. It forms a non-functional, off-pathway, double-ring apoptosome under high protein concentration or high levels of dATP. The auto-inhibited Dark monomer recruits Dronc zymogen to form an unsealed single-ring Dark/Dronc complex, within which Dronc is activated. After cleavage, the dimeric Dronc caspase domains are released from the complex, resulting in a double-ring post-activation Dark/Dronc-CARD complex.

Activation of an initiator caspase is widely believed to depend on its association with a multimeric protein complex called the apoptosome (26). This has been proven true in both *C. elegans* and mammals (27–29). Under homeostatic conditions, the Apaf-1 ortholog CED-4 is sequestered by CED-9 in *C. elegans*, unable to activate the initiator caspase CED-3 (30, 31); Apaf-1 exists as an auto-inhibited monomer, unable to activate caspase-9 (14). Upon apoptotic stimuli, EGL-1 binds to CED-9, releasing CED-4 to form an octameric CED-4 apoptosome (32), whereas mitochondria-released cytochrome c induces formation of the Apaf-1 apoptosome in the presence of ATP or dATP (14). The fully assembled CED-4 and Apaf-1 apoptosome recruit CED-3 and caspase-9, respectively, leading to their activation (27–29).

In sharp contrast to CED-4 and Apaf-1, the auto-inhibited Dark monomer in *Drosophila* directly binds Dronc and mediates its activation through the formation of an unsealed single-ring (13), obviating the need for a pre-assembly step for initiator caspase activation. Notably, the unsealed single ring of Dark is different from the Dark apoptosome. This finding is consistent with the observation that Dronc is continuously processed in healthy S2 cells (33). Under these circumstances, the detrimental proteolytic activity of Dronc is likely mitigated by cellular caspase inhibitors such as DIAP, preventing unwanted apoptosis.

Based on our structural and biochemical results, we propose an updated model for the activation of Dark and Dronc (Fig. 5). In homeostatic cells, Dark exists mainly as a relatively unstable, auto-inhibited monomer in the cytoplasm. Under high protein concentration or high dATP levels, Dark may form a double-ring apoptosome, which represents a non-functional, off-pathway complex. Dronc exists as an inactive zymogen and undergoes continuous DIAP-mediated ubiquitination and proteasome degradation. During apoptosis, the RHG proteins competitively bind to DIAP thereby releasing the Dronc zymogen. The released Dronc interacts with the auto-inhibited Dark through CARD/CARD and CARD/WD1 interactions, leading to the assembly of an unsealed single-ring Dark/Dronc complex, within which Dronc undergoes autocatalytic activation to form catalytic dimers. The double-ring Dark/Dronc-CARD complex (13) may represent the post-activation state. These findings shed light on the mechanisms of apoptosis initiation in *Drosophila*. Future research endeavors should focus on *in vivo* experiments to substantiate these conclusions derived from *in vitro* investigations.

## Materials and Methods

**Protein Expression and Purification.** The full-length cDNA of *D. melanogaster* Dark was subcloned into pFastBac vector (Invitrogen) with a C-terminal 6× His tag and overexpressed using the Bac-to-Bac baculovirus system (Invitrogen). WT Dark and mutant Dark (D333A) were overexpressed in Sf21 insect cells (Invitrogen) using the Sf-900TM II SFM medium (Gibco). Forty-eight hours after viral infection, cells were collected and homogenized in the lysis buffer containing 25 mM Tris (pH 8.0), 150 mM NaCl, and protease inhibitors. After centrifugation at 41,000 rpm for 60 min, the supernatant was harvested and purified to homogeneity using Ni-NTA affinity column (Qiagen) followed by anion exchange chromatography (Source-15Q, GE Healthcare).

WT Dronc and Dronc (4M) (residues 1 to 450, D113A, E135A, E143A, C318A, E352A) were subcloned into pET-21b with a C-terminal 6xHis tag. WT Dronc was overexpressed in *Escherichia coli* strain BL21(DE3) using the M9 minimal medium. Cells were collected and homogenized in the lysis buffer containing 25 mM Tris (pH 8.0) and 150 mM NaCl. Dronc zymogen was purified to homogeneity as quickly as possible using Ni-NTA affinity column (Qiagen) and anion exchange column (Q Sepharose™ Fast Flow, GE Healthcare). Dronc (4M) was expressed in *E. coli* strain BL21(DE3) and similarly purified.

**Assembly of the Dark/Dronc (4M) Complex.** Purified Dark was incubated with an excess amount of Dronc (4M) in the presence of 1 mM dATP for 2 h at 4 °C and fractionated using size exclusion chromatography (Superose™ 6 increase, GE Healthcare) in 25 mM Tris (pH 8.0), 150 mM NaCl, and 5 mM dithiothreitol. Peak fractions around 11.5 mL were collected for cryo-EM studies.

**Cryo-EM Sample Preparation.** Four microliter aliquots of the assembled Dark/Dronc (4M) complex, at a concentration of ~20 μM (Dark monomer) with 0.01% IGEPAL (Sigma), were applied to glow-discharged Quantifoil 300-mesh Au R1.2/1.3 grids. Grids were blotted in a Vitrobot Mark IV (FEI Company) at 8 °C for 2.5 s with 100% humidity and then plunge-frozen in liquid ethane.

Before the cryo-EM sample preparation, Dark (D333A) after anion-exchange chromatography is applied to Superose™ 6 increase (GE Healthcare). The fractions around 16 mL were collected as Dark (D333A) monomer and concentrated. Four microliter aliquots of the Dark (D333A) monomer, at a concentration of ~15 μM with 0.01% IGEPAL (sigma), were applied to glow-discharged graphene-covered Quantifoil 300-mesh Au R1.2/1.3 grids. Grids were blotted using a Vitrobot Mark IV (FEI Company) at 8 °C for 3 s with 100% humidity and then plunge-frozen in liquid ethane.

**Cryo-EM Imaging and Image Processing.** Cryo-EM images were recorded automatically on an FEI Titan Krios electron microscope operating at 300 kV equipped with a K2 Summit detector (Gatan Company). A total of 2,771 and 4,949 micrographs were collected for the Dark/Dronc (4M) complex and the Dark monomer, with a pixel size of 0.97 Å, defocus values between 1.5 and

2.5  $\mu$ m, a total dose of approximately 50 e $^{-\text{Å}}{}^2$ , and an exposure time of 2.56 s. The 32 movie frames of each micrograph were motion corrected by MotionCor2 and binned twofold. CTF parameters of the resulting micrographs were estimated using cryoSPARC v4 (34).

After auto-picking using a template picker, the initial particle stack for the Dark/Dronc (4M) complex was subjected to two-dimensional (2D) classification using cryoSPARC v4. The resulting 153,199 particles from selected 2D averages were subjected to ab initio reconstruction. The particles were separated into two good classes, one containing 27.1% (33,153 particles, double-layered ring) and the other containing 72.9% (89,973 particles, single-layered, unsealed ring). The two classes were subjected to non-uniform refinement with D8 and C1 symmetry. The double-ring structure represents the Dark apoptosome and the unsealed single-ring is the Dark/Dronc (4M) complex. The particle stacks from the latter class were then subjected to 3D classification. One class of hexamer, two classes of heptamer, and one class of octamer were identified, accounting for 68.9%, 10.1%, 11.5%, and 9.5% of total particles, respectively. Each class was further classified to remove bad particles and the final particle stacks (31,849 particles for hexamer, 7,436 for heptamer 1, 8,458 particles for heptamer 2, and 2,710 particles for octamer) were subjected to non-uniform and local refinement in cryoSPARC v4 to average resolutions of 4.6  $\text{\AA}$ , 6.4  $\text{\AA}$ , 6.2  $\text{\AA}$ , and 7.0  $\text{\AA}$ , respectively.

For the Dark (D333A) monomer, 2,357,033 particles were auto-picked using a template picker in cryoSPARC v4. In order to obtain a good reference, initial particle stack was subjected to 2D classification. Then, 138,750 good particles with strong features were selected and subjected to ab initio reconstruction, which separated particles into two bad classes and one good class. The particles from the good class were imported to Relion 3.1 for 3D classification. The resulting 32,845 particles were bin1 extracted and subjected to non-uniform (NU) refinement to generate a good reference. After obtaining good and bad references, 2,357,033 auto-picked particles were directly subjected to heterogeneous refinement. The best class was NU refined and subjected to a second round of heterogeneous refinement to remove bad particles. Finally, 105,018 particles were NU and local refined to generate a map at 3.9  $\text{\AA}$  resolution.

**Model Building and Refinement.** For the Dark/Dronc (4M) complex, the cryo-EM structure of the Dark/Dronc-CARD complex (PDB code: 3J9K) was docked into the overall maps using COOT (35) and fitted into EM density using CHIMERA (36). For the inactive Dark (D333A) monomer, the cryo-EM structure of Dark (D333A) monomer from the Dark apoptosome (PDB code: 3J9L) was used for model building using COOT and CHIMERA. WD2 was auto-built by ModelAngelo (37). Initial structural refinement was carried out using PHINEX (38).

**Assembly Assay of the Dark/Dronc (4M) Complex.** First, 3.64  $\mu$ M WT Dark monomer or pre-assembled Dark apoptosome were incubated with 3.85  $\mu$ M Dronc (4M) for 2 h at 4  $^{\circ}\text{C}$  and further purified using SEC (Superose™ 6 increase, GE Healthcare). All peak fractions were visualized on SDS-PAGE followed by Coomassie blue staining.

**dATP Concentration Gradient Assay.** Ten micrometer Dark (WT) was incubated with 0, 0.02, 1, and 5 mM dATP for 2 h at 4  $^{\circ}\text{C}$  before loading onto Superose™

6 increase (GE Healthcare). All peak fractions were visualized on SDS-PAGE followed by Coomassie blue staining.

**Dronc Activation Assay.** Reactions were carried out for 1 h at room temperature in an assay buffer containing 25 mM Tris (pH 8.0), 150 mM NaCl, and 5 mM DTT. The concentrations of Dark (WT) and Dronc zymogen were both 0.73  $\mu$ M in each reaction. Dronc autocatalytic cleavage was visualized on SDS-PAGE followed by Coomassie blue staining.

**Negative Staining EM.** Four microliter of the freshly prepared sample was loaded onto a glow-discharged (PELCO) carbon-coated copper grid (300 mesh, Zhongjingkeyi Technology) and incubated for 2 min. The excess sample liquid was removed using a filter paper and then the grid was stained using a droplet of 3% uranyl acetate for 10 s. The staining process was repeated three times and the third staining process was carried out with one extra minute. Finally, the excess staining buffer was removed using a filter paper, and the grid was dried at room temperature. The prepared grids were observed on a FEI Tecnai Spirit with iCorr microscope operating at 120 kV, using a FEI Eagle 4 k CCD camera at a nominal magnification of 52,000.

**LC-MS/MS.** Purified Dark protein was sent to identify the bound nucleotide through LC-MS/MS. The ACQUITY UPLC H-Class system was coupled a 6500plus QTrap mass spectrometer (AB SCIEX), equipped with a heated electrospray ionization (HESI) probe. Extracts were separated by a Syngene Hydro-RP column (2.0  $\times$  100 mm, 2.5  $\mu$ m, Phenomenex). A binary solvent system was used, in which mobile phase A consisted of 2 mM Trisobutylamine adjusted with 5 mM acetic acid in water and mobile phase B of methanol. An 8-min gradient with flow rate of 500  $\mu$ L/min was used as follows: 0 to 0.8 min at 5% B; 0.8 to 6 min, 5 to 45% B; 6.1 to 6.9 min, 98% B; 7.0 to 8 min, 5% B. Column chamber and sample tray were held at 35  $^{\circ}\text{C}$  and 10  $^{\circ}\text{C}$ , respectively. Data were acquired in multiple reaction monitor (MRM) mode. The nebulizer gas (Gas1), heater gas (Gas2), and curtain gas were set at 55, 55, and 35 psi, respectively. The ion spray voltage was  $-4,000$  V in negative ion mode. The optimal probe temperature was determined to be 400  $^{\circ}\text{C}$ . The SCIEX OS 1.6 software was applied for metabolite identification and peak integration.

**Data, Materials, and Software Availability.** The atomic models are available through the PDB with accession codes: 8Y6P (39) and 8Y6Q (40). All cryo-EM reconstructions are available through the EMDB with accession codes: EMD-38994 (41) and EMD-38995 (42).

**ACKNOWLEDGMENTS.** This work was financially supported by Beijing Frontier Research Center for Biological Structure, Tsinghua-Peking Center for Life Sciences, and Westlake University. Y.L. was supported by fellowships from the Beijing Advanced Innovation Center for Structural Biology and Tsinghua-Peking Center for Life Sciences. We thank the Tsinghua University Branch of China National Center for Protein Sciences (Beijing) for the cryo-EM facility and the computational facility support. We thank the Metabolomics Facility Center of Metabolomics and Lipidomics in National Protein Science Technology Center of Tsinghua University for LC-MS/MS experiments.

1. N. N. Danial, S. J. Korsmeyer, Cell death: Critical control points. *Cell* **116**, 205–219 (2004).
2. Y. Fuchs, H. Steller, Programmed cell death in animal development and disease. *Cell* **147**, 742–758 (2011).
3. H. R. Horvitz, Worms, life, and death (Nobel lecture). *Chem Biochem* **4**, 697–711 (2003).
4. S. J. Riedl, Y. Shi, Molecular mechanisms of caspase regulation during apoptosis. *Nat Rev Mol Cell Biol* **5**, 897–907 (2004).
5. N. Yan, Y. Shi, Mechanisms of apoptosis through structural biology. *Annu Rev Cell Dev Biol* **21**, 35–56 (2005).
6. J. Chai, Y. Shi, Apoptosome and inflammasome: Conserved machineries for caspase activation. *Natl Sci Rev* **1**, 101–118 (2014).
7. B. A. Hay, Understanding IAP function and regulation: A view from Drosophila. *Cell Death Differ* **7**, 1045–1056 (2000).
8. R. Wilson *et al.*, The DIAP1 RING finger mediates ubiquitination of Dronc and is indispensable for regulating apoptosis. *Nat Cell Biol* **4**, 445–450 (2002).
9. J. Chai *et al.*, Molecular mechanism of Reaper-Grim-Hid-mediated suppression of DIAP1-dependent Dronc ubiquitination. *Nat Struct Mol Biol* **10**, 892–898 (2003).
10. H. Kanuka *et al.*, Control of the cell death pathway by Daf-1, a Drosophila Apaf-1/CED-4-related caspase activator. *Mol Cell* **4**, 757–769 (1999).
11. A. Rodriguez *et al.*, Dark is a Drosophila homologue of Apaf-1/CED-4 and functions in an evolutionarily conserved death pathway. *Nat Cell Biol* **1**, 272–279 (1999).
12. L. Zhou, Z. Song, J. Tittel, H. Steller, HAC-1, a Drosophila homolog of APAF-1 and CED-4 functions in developmental and radiation-induced apoptosis. *Mol Cell* **4**, 745–755 (1999).
13. Y. Pang *et al.*, Structure of the apoptosome: Mechanistic insights into activation of an initiator caspase from Drosophila. *Genes Dev* **29**, 277–287 (2015).
14. P. Li *et al.*, Cytochrome c and dATP-dependent formation of Apaf-1/caspase-9 complex initiates an apoptotic protease cascade. *Cell* **91**, 479–489 (1997).
15. N. Yan *et al.*, Structure and activation mechanism of the Drosophila initiator caspase Dronc. *J Biol Chem* **281**, 8667–8674 (2006).
16. X. Liu, C. N. Kim, J. Yang, R. Jemmerson, X. Wang, Induction of apoptotic program in cell-free extracts: Requirement for dATP and cytochrome c. *Cell* **86**, 147–157 (1996).
17. H. Zou, W. J. Henzel, X. Liu, A. Lutschg, X. Wang, Apaf-1, a human protein homologous to *C. elegans* CED-4, participates in cytochrome c-dependent activation of caspase-3. *Cell* **90**, 405–413 (1997).
18. L. Dorstyn, K. Mills, Y. Lazebnik, S. Kumar, The two cytochrome c species, DC3 and DC4, are not required for caspase activation and apoptosis in Drosophila cells. *J Cell Biol* **167**, 405–410 (2004).
19. L. Dorstyn *et al.*, The role of cytochrome c in caspase activation in *Drosophila melanogaster* cells. *J Cell Biol* **156**, 1089–1098 (2002).
20. X. Yu, L. Wang, D. Acehan, X. Wang, C. W. Akey, Three-dimensional structure of a double apoptosome formed by the Drosophila Apaf-1 related killer. *J Mol Biol* **355**, 577–589 (2006).
21. T. C. Cheng *et al.*, A near-atomic structure of the dark apoptosome provides insight into assembly and activation. *Structure* **25**, 40–52 (2017).
22. S. Yuan *et al.*, Structure of the Drosophila apoptosome at 6.9  $\text{\AA}$  resolution. *Structure* **19**, 128–140 (2011).
23. S. J. Riedl, W. Li, Y. Chao, R. Schwarzenbacher, Y. Shi, Structure of the apoptotic protease-activating factor 1 bound to ADP. *Nature* **434**, 926–933 (2005).

24. M. Zhou *et al.*, Atomic structure of the apoptosome: Mechanism of cytochrome c- and dATP-mediated activation of Apaf-1. *Genes Dev.* **29**, 2349–2361 (2015).
25. T. W. Traut, Physiological concentrations of purines and pyrimidines. *Mol. Cell Biochem.* **140**, 1–22 (1994).
26. Y. Shi, Caspase activation, inhibition, and reactivation: A mechanistic view. *Protein Sci.* **13**, 1979–1987 (2004).
27. X. Yang, H. Y. Chang, D. Baltimore, Essential role of CED-4 oligomerization in CED-3 activation and apoptosis. *Science* **281**, 1355–1357 (1998).
28. N. Yan, Y. Xu, Y. Shi, 2:1 Stoichiometry of the CED-4–CED-9 complex and the tetrameric CED-4: Insights into the regulation of CED-3 activation. *Cell Cycle* **5**, 31–34 (2006).
29. J. Rodriguez, Y. Lazebnik, Caspase-9 and APAF-1 form an active holoenzyme. *Genes Dev.* **13**, 3179–3184 (1999).
30. F. Chen *et al.*, Translocation of *C. elegans* CED-4 to nuclear membranes during programmed cell death. *Science* **287**, 1485–1489 (2000).
31. A. M. Chinnaiyan, K. O'Rourke, B. R. Lane, V. M. Dixit, Interaction of CED-4 with CED-3 and CED-9: A molecular framework for cell death. *Science* **275**, 1122–1126 (1997).
32. L. del Peso, V. M. González, G. Núñez, *Caenorhabditis elegans* EGL-1 disrupts the interaction of CED-9 with CED-4 and promotes CED-3 activation. *J. Biol. Chem.* **273**, 33495–33500 (1998).
33. I. Muro, B. A. Hay, R. J. Clem, The Drosophila DIAP1 protein is required to prevent accumulation of a continuously generated, processed form of the apical caspase DRONC. *J. Biol. Chem.* **277**, 49644–49650 (2002).
34. A. Punjani, J. L. Rubinstein, D. J. Fleet, M. A. Brubaker, cryoSPARC: Algorithms for rapid unsupervised cryo-EM structure determination. *Nat. Methods* **14**, 290–296 (2017).
35. P. Emsley, K. Cowtan, Coot: Model-building tools for molecular graphics. *Acta Crystallogr. D Biol. Crystallogr.* **60**, 2126–2132 (2004).
36. E. F. Pettersen *et al.*, UCSF Chimera—a visualization system for exploratory research and analysis. *J. Comput. Chem.* **25**, 1605–1612 (2004).
37. K. Jamali *et al.*, Automated model building and protein identification in cryo-EM maps. bioRxiv [Preprint] (2023). <https://doi.org/10.1101/2023.05.16.541002> (Accessed 16 May 2023).
38. P. D. Adams *et al.*, PHENIX: Building new software for automated crystallographic structure determination. *Acta Crystallogr. D Biol. Crystallogr.* **58**, 1948–1954 (2002).
39. L. Tian, Y. Li, Y. Shi, Structure of the auto-inhibited Dark monomer. PDB. <https://www.rcsb.org/structure/8Y6P>. Deposited 3 February 2024.
40. L. Tian, Y. Li, Y. Shi, Structure of the Dark/Dronc complex. PDB. <https://www.rcsb.org/structure/8Y6Q>. Deposited 3 February 2024.
41. L. Tian, Y. Li, Y. Shi, Structure of the auto-inhibited Dark monomer. EMDB. <https://www.ebi.ac.uk/emdb/EMD-38994>. Deposited 3 February 2024.
42. L. Tian, Y. Li, Y. Shi, Structure of the Dark/Dronc complex. EMDB. <https://www.ebi.ac.uk/emdb/EMD-38995>. Deposited 3 February 2024.